# Heterogeneous reactions of HOI, ICl and IBr on sea salt and sea salt proxies

**ARTICLE** *in* PHYSICAL CHEMISTRY CHEMICAL PHYSICS · JULY 2007

Impact Factor: 4.49 · DOI: 10.1039/b700829e · Source: PubMed

# Heterogeneous reactions of HOI, ICl and IBr on sea salt and sea salt proxies

C. F. Braban,[a] J. W. Adams,[a] D. Rodriguez,†[a] R. A. Cox,[a] J. N. Crowley[b] and G. Schuster[b]

*Received 18th January 2007, Accepted 27th March 2007*
*First published as an Advance Article on the web 26th April 2007*
**DOI: 10.1039/b700829e**



The heterogeneous chemistry of HOI, ICl and IBr on sea salt and sea salt proxies has been studied at 274 K using two experimental approaches: a wetted wall flow tube coupled to an electron impact mass spectrometer (WWFT-MS) and an aerosol flow tube (AFT) coupled to a differential mobility analyser (DMA) and a chemical ionisation mass spectrometer (CIMS). Uptake of all three title molecules into bulk aqueous halide salt films was rapid and controlled by gas phase diffusion. Uptake of HOI gave rise to gas-phase ICl and IBr, with the latter being the predominant product whenever $Br^-$ was present. Only partial release of IBr was observed due to high solubility of dihalogens in the film. ICl uptake gave the same yield of IBr as HOI uptake. Uptake of ICl on NaBr aerosol was accommodation limited with $\alpha = 0.018 \pm 0.004$ and gas phase IBr product has a yield of $0.6 \pm 0.3$. The results show that HOI can act as a catalyst for activation of bromine from sea-salt aerosols in the marine boundary layer, *via* the reactions: $HOI_{aq} + Cl^-_{aq} + H^+_{aq} \rightarrow ICl_{aq} + H_2O_l$ and $ICl_{aq} + Br^-_{aq} \rightarrow IBr_{aq} + Cl^-_{aq}$.

## 1. Introduction

Most iodine in the marine environment is emitted in the form of gas-phase biogenic organic iodine compounds. Several iodocarbons have relatively short photochemical lifetimes, resulting in the release of gas phase I atoms which react mainly with ozone to form the IO radical. IO has been observed at ppt levels at several locations in the marine boundary layer (MBL) at mid latitudes[1,2] and in the polar troposphere.[3] Reactive inorganic halogen species such as IO in the marine boundary layer can directly influence levels of oxidants such as ozone. The IO radical can react with $HO_2$ or $NO_2$ in the gas phase, leading to the formation of HOI and $IONO_2$ (R1, R2):

$$IO + HO_2 \rightarrow HOI + O_2 \quad (R1)$$

$$IO + NO_2 + M \rightarrow IONO_2 + M \quad (R2)$$

HOI can reform IO *via* photolysis[4,5] contributing to ozone destruction *via* R3–R5.

$$HOI + h\nu \rightarrow OH + I \quad (R3)$$

$$I + O_3 \rightarrow IO + O_2 \quad (R4)$$

$$OH + O_3 \rightarrow HO_2 + O_2 \quad (R5)$$

In addition to gas phase processes, both HOI and $IONO_2$ may undergo heterogeneous reactions on aerosol surfaces. Indeed, the conversion of $IONO_2$ to HOI can occur by hydrolysis on aqueous particles (R6).

$$IONO_{2aq} + H_2O_{aq} \rightarrow HOI_{aq} + HNO_{3aq} \quad (R6)$$

Despite its short photochemical lifetime, models predict HOI to be one of the most abundant reservoirs of inorganic iodine in the MBL and therefore its heterogeneous reactions could be very significant.[6–8]

Potential heterogeneous loss processes for HOI in the MBL include its reaction with acidified, aqueous halide solutions (*e.g.*, sea salt aerosol) to form di-halogens:

$$HOI_{aq} + Cl^-_{aq} + H^+_{aq} \rightarrow ICl_{aq} + H_2O_l \quad (R7)$$

or

$$HOI_{aq} + Br^-_{aq} + H^+_{aq} \rightarrow IBr_{aq} + H_2O_l \quad (R8)$$

The fate of the ICl and IBr products depends on their solubilities and on the rates of aqueous phase interconversion reactions. As the molar ratio of chlorine to bromine in sea-water is ~658, R7 may be expected to dominate, resulting in $ICl_{aq}$ formation. The release of ICl to the gas phase would then constitute an iodine-mediated chlorine activation mechanism, whereby I atoms are recycled.

$$ICl + h\nu \rightarrow I + Cl \quad (R9)$$

This has been discussed by McFiggans *et al.*,[7] who considered the rate of atomic chlorine activation to be related to the rate of attachment of HOI at the aerosol surface, given by:

$$\frac{d[ICl_g]}{dt} = \frac{f\gamma\bar{c}A}{4}[HOI] \quad (1)$$

where $A$ is the aerosol surface area of the sea salt, $f$ is the fractional conversion of HOI to gaseous ICl, $\gamma$ is the uptake coefficient and $\bar{c}$ is the mean speed of the HOI gas molecules.

[a] *Department of Chemistry, University of Cambridge, Lensfield Rd, Cambridge, UK CB2 1EW*
[b] *Max-Planck-Institut für Chemie, Division of Atmospheric Chemistry, Postfach 3060, 55020 Mainz, Germany*
† Present address: Departamento de Química Física, Facultad de Ciencias del Medio Ambiente, Universidad Castilla-La Mancha Avda. Carlos III s/n 45071 Toledo, Spain.

 

The presence of aerosol bromide may cause reaction R10 to compete with ICl release, switching a chlorine activation mechanism into bromine activation, following release of bromine either as IBr or $Br_2$, leading to $f \ll 1$. This process is important since Br is efficient for depletion of $O_3$ in the marine boundary layer.[9,10] Inorganic bromine in aged sea salt aerosol is frequently depleted in bromide relative to conservative tracers of seawater composition, and in fresh sea salt aerosol.[10]

$$ICl_{aq} + Br^-_{aq} \rightarrow IBr_{aq} + Cl^-_{aq} \qquad (R10)$$

$$IBr + h\nu \rightarrow I + Br \qquad (R11)$$

The value of $f$ was estimated to be 0.5 for a mixed-age MBL aerosol assemblage, by analogy with the efficiency for BrCl activation by HOBr.[3] Note also, that HOI can be formed at night by the hydrolysis of $IONO_2$ (R6). The likelihood of HOI reacting with sea-salt aerosol is significantly larger than during the day, as photolysis stops at dusk. If ICl is released to the gas phase at nightime, it may accumulate in the absence of photolysis, and there is a possibility that ICl can re-enter the sea salt aerosol and participate in the aqueous halide chemistry, *via* the reverse of reaction R7. For this reason the heterogeneous reactions of both HOI and ICl with sea salt aerosol need to be understood.

It is noted that the above reactions are a highly simplified representation of the aqueous phase equilibrium chemistry that occurs in the aerosol. The linked gas phase and heterogeneous chemical cycles of HOX (X = Cl, Br or I) and formation of gas phase molecular halogens have been described in detail previously[7,10–12] and have been the subject of several laboratory and modeling studies.[13–20] Two parameters that have significant impact on the role of HOI in the MBL are its rate of processing by marine aerosols, and the identity of the photolabile halogens that can be released to the gas-phase.

Marine aerosol includes both submicron (accumulation mode) and supermicron (coarse mode) particles. They consist both of inorganic ions and organic compounds present in seawater, and additional components formed by chemical reactions during aging. The latter are either taken up from the gas phase or formed by reactions in the aerosol. Fresh sea salt particles are aqueous and have a pH of between 7.5 to 8.5. The pH decreases with time as acidic gases, in particular $SO_2$, are absorbed from the atmosphere. Initial sea salt alkalinity is titrated rapidly and near equilibrium pH established on relatively short timescales.[21] Modeled aged marine aerosol pHs are in the range 4.5–5.4 for super micron particles, and 2.6–5.3 for submicron particles.[22] The aerosol pH is also regulated by the HCl partitioning,[23] which is, in turn, determined by the sulfate content of the aerosol. Since the aqueous phase reactions following HOI uptake involve $H^+$ ions, processing rates are likely to depend on pH.

In this work, we investigated the uptake of both HOI and ICl onto aqueous salt surfaces, extending a small body of laboratory studies using solid halide surfaces.[13,14,19] A summary of these studies is presented in Table 1. Most of these studies were performed using low relative humidities with either dry or frozen salts as substrates. They show that both ICl and IBr are released following HOI uptake on solid surfaces containing sea salt, and that when $Br^-$ is present ICl uptake forms IBr. The rate of HOI uptake appears to be faster than ICl.

In the present work two experimental techniques have been used: a wetted wall flow tube system (WWFT) and an aerosol flow tube coupled to a chemical ionisation mass spectrometer. With the former technique uptake studies of HOI, ICl and IBr were carried out onto bulk aqueous film substrates. With the AFT-CIMS it was possible to study the uptake on to aerosols of ICl as a proxy for HOI, based on the assumption that R7 is fast. Experiments were performed mostly using sodium bromide aerosol, in order to ascertain if the release of IBr was quantitative. The advantage of the aerosol experiment is that the process is not strongly influenced by volume and mass transfer effects given the small volume of the particles. The pH

**Table 1** Summary of literature data for HOI and ICl uptake onto salt and salt proxies

| | | | HOI | | | ICl | | | |
|---|---|---|---|---|---|---|---|---|---|
| Substrate | RH | $T$/K | $\gamma$ | Products | Yield | $\gamma$ | Products | Yield | Ref. |
| Seasalt fresh | 0 | 298 | 0.061 | IBr, ICl | f(t) | 0.0012 | IBr | 0.3 | 13 |
| Aged | 0 | 298 | 0.014 | ICl IBr | 0.3 | — | — | — | 13 |
| Seasalt fresh | 11 | 278 | 0.02 | none | — | — | — | — | 13 |
| NaBr fresh | 0 | 298 | 0.034 | IBr | 1 | 0.0068 | IBr | 1 | 13 |
| Aged | 0 | 298 | 0.008 | IBr | 0.19 | — | IBr | 0.7 | 13 |
| NaBr fresh | 11 | 278 | 0.008 | IBr | — | — | — | — | 13 |
| NaCl fresh | 0 | 298 | 0.016 | ICl | 0.1 | $<10^{-4}$ | — | — | 13 |
| Aged | 0 | 298 | 0.007 | ICl | 0.1 | — | — | — | 13 |
| NaCl fresh | 11 | 278 | 0.008 | ICl | 0.1 | — | — | — | 13 |
| NaOH fresh | 0 | 298 | 0.016 | none | 0 | 0.0034 | None | — | 13 |
| Aged | 0 | 298 | 0.0022 | none | 0 | — | — | — | 13 |
| NaOH | 11 | 278 | >0.1 | none | 0 | >0.1 | None | — | 13 |
| NaCl | 0 | 298 | 0.04 | none | | — | — | — | 19 |
| KBr | 0 | 298 | 0.06 | none | | — | — | — | 19 |
| $NaCl/NaBr_{(s)}$ | 0 | 298 | >0.01 | IBr,ICl | 1 | — | — | — | 14 |
| | 0 | 243 | >0.01 | IBr,ICl | 1 | — | — | — | 14 |
| Frozen film NaCl/NaBr | 0 | 243 | >0.01 | IBr,ICl | 1 | >0.01 | IBr | 1 | 14 |
| $H_2SO_4$ | 0 | 298 | >0.04 | IBr,ICl | 1 | — | — | — | 14 |
| | 0 | 243 | >0.04 | IBr,ICl | 1 | — | — | — | 14 |

dependence of product release from salt solutions is considered and the implications of the results are discussed in the context of bromide and chloride depletion from marine aerosols.

## 2. Experimental

### 2.1 Wetted wall flow tube-electron impact mass spectrometer (WWFT-EIMS)

The interaction of HOI and ICl with seawater and seawater proxies was studied using a vertically mounted wetted wall flow tube coupled to a mass spectrometer for gas-phase analysis. Two similar but independent set-ups were used located at the University of Cambridge (UCAM) and Max-Planck-Institute (MPI), Mainz (Germany). The MPI apparatus has been described in detail previously[15,24] and only pertinent details are given here. The MPI experiments, focussing on the uptake of ICl only, were conducted at 278 and 293 K and at a range of pressures (approximately 20–200 Torr). The mean linear velocity of gas flowing in the 1.55 cm diameter flow tube varied between 30 and 130 cm $s^{-1}$, according to the flow rate ($\approx$300–700 sccm) and pressure. Reynolds numbers were typically between 10 and 20, with entrance lengths to establish laminar flow of 1–2 cm. The thickness and speed of the liquid film were calculated as described previously[24] to be $\approx$100 μm and 3–4 cm $s^{-1}$, respectively. The halogen gases diluted in He were introduced into the reactor *via* a moveable sliding injector.

The UCAM WWFT was similar to the Mainz equipment described above. The cylindrical reactor had a larger internal diameter (2.4 cm), and a slower speed ($\sim$0.2 cm $s^{-1}$) and smaller thickness ($\sim$25 μm) of the aqueous film. The pressure in the flow tube was in the range 5–20 Torr and at the temperature of 274 K, in order to minimise the water vapour pressure. The total gas flow in the flow tube was between 800–1000 $cm^{-3}$ (STP) $min^{-1}$ resulting in linear velocities of between 150–200 cm $s^{-1}$. The relative humidity (RH) was maintained at that of the saturated salt solution by maintaining a flow of water saturated He. The gas is sampled into the mass spectrometer (Extrel Merlin QMS) at the base of the flow tube through an elevated sampling port. The mass spectrometer was operated with electron impact ionisation in these experiments. The mass spectrometer has two-stage pumping with ion deflection. HOI, ICl and IBr were measured as the parent positive ions: $m/z$ 144, 162 and 206, respectively.

The aqueous solutions studied were water, sea salt and sea salt proxy solutions. These were prepared by the dissolution of salts in pre-acidified, distilled water. The compositions are summarised in Table 2. The pH 2 solutions were prepared by addition of $H_2SO_4$ or HCl (no difference was observed in the experimental results between the two acids). The pH 5.5 solution was prepared using a $KHC_8O_4H_4$/KOH buffer, pH 7.5 using $KH_2PO_4$/KOH buffer. Solutions of pH 10 were prepared using $NaOH_{(aq)}$. Other salt solutions had neutral pH.

HOI was prepared *in situ via* the reaction of O atoms (generated in a microwave discharge) with $C_2H_5I$ or $C_3H_7I$ in a flow of He at reduced pressure. HOI concentrations in the range (6–80) $\times$ $10^{10}$ $cm^{-3}$ were obtained in this way, but it proved impossible to produce sufficient HOI for experiments at pressures $>$76 Torr. The mass spectrometer signal for HOI ($m/z$ 144) was cross calibrated with the product species ICl ($m/z$ 162) and IBr ($m/z$ 206) following reaction of HOI on a solid salt surface containing both chloride and bromide.

**Table 2** Summary of HOI, ICl and IBr uptake studies with wetted wall flow tube system

| | | Film surface composition/M | | | | | |
|---|---|---|---|---|---|---|---|
| Reactant | Temp/K | $[Cl^-]$ | $[Br^-]$ | pH | $\gamma/10^{-3}$ | Diffusion limited? | Gas-phase products |
| HOI | 274 | 0 | 0 | Unadjusted | 2.0 ± 0.2[b] | Y[b] | no |
| | | 2 | 0 | 2 | 2.2 ± 0.6 | Y | ICl |
| | | 2 | 0.01 | 2 | 1.8 ± 0.2 | Y | ICl,IBr |
| | | 2 | 0.01 | Unadjusted | 2.2 ± 0.6 | | IBr |
| | | 2 | 0.1 | 2 | 2.2 ± 0.2 | Y | IBr |
| | | 2 | 0.1 | 5.5[a] | 2.2 ± 0.2 | | IBr |
| | | 0 | 0.1 | 2 | 1.70 | Y | IBr |
| ICl(*UCAM*[c]) | 274 | 0 | 0 | Unadjusted | 3.5 ± 0.5[b] | Y[b] | no |
| | | 2 | 0.003 | 2 | 2.5 ± 0.1 | Y | IBr |
| | | | | 5.5[a] | 2.6 ± 0.2 | | IBr |
| | | | | 7.5[a] | 2.6 ± 0.1 | | IBr |
| | | | | 10 | 2.9 ± 0.2 | | no |
| | | 0 | 2 | Unadjusted | 2.6 | Y | IBr |
| ICl (*MPI*) | 278 | 0 | 0 | Unadjusted | 0.66–2.0[d] | Y | — |
| | 278 | 0 | 2 | 2 | 0.62–1.4[d] | Y | — |
| | 293 | 0 | 0 | Unadjusted | 0.5–0.6[d] | N | — |
| | 293 | 0 | 2 | 2 | 0.6–1.6[d] | Y | — |
| IBr(*UCAM*[c]) | 274 | 0 | 0 | Unadjusted | 1.8 ± 0.2[b] | N[b] | no |
| | | 2 | 0.003 | 2 | 2.0 ± 0.2 | Y | no |
| | | | | Unadjusted | | | |

[a] Buffered solution. [b] First order kinetics not observed; initial $\gamma$ at short exposure time given. [c] All UCAM ICl IBr uptakes at 13 Torr nominal pressure. [d] Range of $\gamma$ values for different total pressure.

 

Molecular $I_2$ is generated in the microwave source in addition to HOI, and was taken up onto the salt surface. A small constant amount of IBr from $I_2$ reaction was accounted for in calculating IBr yields from HOI. ICl and IBr in the WWFT experiments were sampled from storage bulbs that were prepared as follows. Following purification by repetitive freeze–pump–thaw cycles, known pressures of the gases were mixed with an appropriate pressure of helium to give the desired dilution. The mass spectrometer was calibrated for ICl and IBr using accurately diluted mixtures of the halogens in He.

### 2.2 Aerosol flow tube-chemical ionisation mass spectrometry (CIMS) system

The aerosol flow tube-chemical ionization mass spectrometer system (AFT-CIMS) is shown schematically in Fig. 1. With this system it is possible to generate a constant flow of aerosol particles at controlled relative humidity (RH), determine the number/particle size distribution of the particles, and hence the surface area of the particles, and measure gas uptake on this aerosol.

Aerosol is produced in the atomizer (TSI 3076) from salt solutions with concentrations between 0.1 and 1 M. If dry particles were to be studied, the aerosol flow was passed through a custom-built diffusion dryer (residence time $\sim$30 s). A fraction of the aerosol flow is mixed with two flows of nitrogen, one of which is dry and the other saturated with water. The ratio of these flows is varied in order to set the RH of the aerosol flow. The flow passes through a thermostatted-conditioning region (residence time $\sim$1–2 min). Subsequently, the flow is split into three: a fraction is sampled by a differential mobility analyser (DMA, Hauke, model FCE 08/A) in order to determine the particle size distribution; a fraction is pumped through the AFT; and the excess flow is vented. The DMA system is described more fully in section 2.4 and in Badger *et al.*[25] A commercial hygrometer probe (Vaisala) is inserted in the system at the point where the aerosol flow enters the AFT. The AFT itself is a vertically mounted 85 cm, 3.4 cm id Pyrex flow tube that is thermally jacketed. The outlet is connected to the first pumping stage of the CIMS. The experimental temperature was 274 K in all the experiments reported here, and pressure in the flow tube was atmospheric ($\sim$750–760 Torr). The flow rate was constant and is set by the pressure drop across a critical orifice between the AFT and the CIMS region. The CIMS region is evacuated using a rotary vacuum pump coupled with a Roots pump. Two different diameter orifices were used in the course of the experiments: 0.5 mm and 0.2 mm that led to flows of 3000 sccm and 600 sccm in the AFT, respectively, as measured with a calibrated flow meter in the absence of aerosol. Laminar flow conditions exist in both cases. Kinetic measurements are not made in the top and bottom 20 cm section of the flow tube, to allow for laminar flow development at the inlet and mixing of the reactive species after injection.

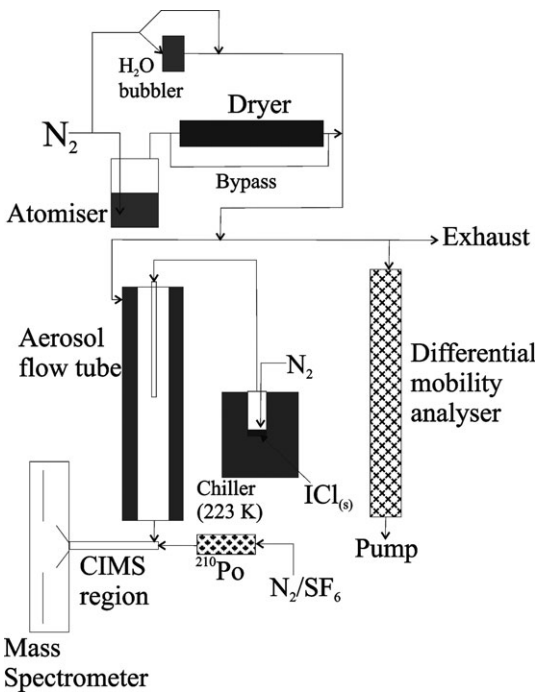


**Fig. 1** Schematic of the aerosol flow tube-CIMS system.

The reactive species in these experiments, $ICl_{(g)}$, was introduced into the flow tube *via* a moveable 3 mm id Pyrex injector tube, which was mounted vertically, concentric with the aerosol flow tube. The $ICl_{(g)}$ was obtained by flowing nitrogen (usually 25 sccm) over the headspace of solid ICl, which was held in a cold finger at 223 K in a non-circulating chiller (Huber CC180). ICl mixing ratios of between 300 and 700 ppb ($0.8–1.7 \times 10^{13}$ molecule $cm^{-3}$) were used. The ICl was stored in the cold finger in the dark at 200 K and was used for only few experiments before replacement.

### 2.3 CIMS detection of ICl and IBr

The reagent and product species were detected using CIMS. $SF_6^-$ and $O_2^-$ were tested as potential reagent ions. Both showed significantly decreased sensitivity in the presence of water vapor, due to the formation of cluster ions. In order to maximize the sensitivity while being able to perform experiments over a full range of relative humidity most experiments were carried out at 274 K. All experiments reported here used $SF_6^-$ as reagent ion, which was produced by flowing $\sim$5 slm $SF_6$ in $N_2$ though a $^{210}$Po radioactive source (StatAttack Ltd). This flow mixed with the flow through the orifice from the AFT *via* a 1/4″ T-union. The mixed flows where then directed down a 1/4″ stainless steel tube which stopped $<$5 mm from the entrance to the mass spectrometer. The ions pass through 2 further stages of pumping before detection. The ICl was observed as the product ion $IClF^-$ ($m/z$ 181) and IBr was observed similarly as $IBrF^-$ ($m/z$ 225).

The sensitivity of the CIMS to ICl was measured by introduction of ICl from a bulb, and found to be 0.15 $\pm$ 0.04 counts $ppb^{-1}$. The detection limit at low RH was $\sim$30 ppb. The cause of the relatively low sensitivity of this CIMS system compared to other CIMS systems in the literature is the design of the current inlet system which leads to significant ion loss between ionization and sampling of ions into the mass spectrometer. However it was found that working with sufficiently large aerosol surface areas, the sensitivity of the system was sufficient to measure uptake kinetics onto halide aerosols.

### 2.4 Differential mobility analysis

During a single scan the DMA measures the aerodynamic particle diameters in the range 20–1000 nm, measurements being made at 35 size bins over a period of about 5 min; between 2 and 4 scans are averaged to obtain the size distribution during a kinetic run. In order to determine the correct surface area for the aerosol at 274 K, the particle size distribution was measured "dry" (RH < 5%, 295 K) in each separate uptake experiment, and then corrected for the RH in the flow tube, using data obtained from separate particle growth studies made using a tandem-DMA set-up, described in Badger *et al.*[25] The measured deliquescence relative humidity of sodium bromide aerosol was 50 ± 3%, in agreement with the literature.[26] The aerosol made from Norwegian sea water showed no deliquescent point in the tandem-DMA experiment, with continuous growth over all relative humidities, in agreement with the AFT-FTIR studies of Cziczo *et al.*,[27] which used a laboratory mixed artificial seawater. Growth factors at RH = 85% were 1.85 and 2.15 for the sodium bromide and sea salt aerosol, respectively. Although no literature data is available for growth of sodium bromide aerosol, the sea salt aerosol growth factor is in good agreement with the only other study of sea salt particle growth found in the literature.[28]

The integrated surface areas used for calculation of the uptake coefficients were obtained from the measured size distribution after correction for humidity change. In the experiments reported here the aerosol surface areas were in the range $1 \times 10^{-4}$–$8 \times 10^{-3}$ cm$^2$ cm$^{-3}$, with the mean area-weighted radius between 100 and 1000 nm.

## 3. Results

### 3.1 Wetted wall flow tube studies

**3.1.1 Data analysis.** HOI, ICl and IBr uptake onto seawater and seawater proxies were studied using the WWFT systems at MPI and UCAM. The experimental pseudo-first order loss coefficient of a trace gas, $k_w$, is calculated from the variation of signal with injector position (eqn (2))

$$[C]_{z_2} = [C]_{z_1} \exp\left(-k_w \frac{\Delta z}{\nu}\right) \quad (2)$$

where $[C]_{z_{1,2}}$ are the trace gas concentrations at injection positions $z_1$ and $z_2$, $\Delta z = z_2 - z_1$, $\nu$ is the gas flow velocity in the tube. The overall experimental uptake coefficient $\gamma_{meas}$ of gas molecules from the gas-phase into a liquid can be considered in terms of a sequence of resistances, including gas-phase diffusion to the interface $\gamma_{diff}$, the mass accommodation coefficient $\alpha$, liquid phase reaction $\gamma_{rxn}$, and/or solvation $\gamma_{sol}$ of the trace gas:

$$\frac{1}{\gamma_{meas}} = \frac{1}{\gamma_{diff}} + \frac{1}{\alpha} + \frac{1}{\gamma_{sol} + \gamma_{rxn}} \quad (3)$$

When one of the parameters becomes rate limiting the expression can be simplified. In the case of most of the WWFT experiments reported here, analysis shows that the uptake coefficients are diffusion limited, *i.e.* transport of the trace gas to the liquid surface was limiting and thus $1/\gamma_{meas} = 1/\gamma_{diff} + 1/\alpha$. Correcting for the geometry of the cylinder $\gamma_{diff}$ is given by:

$$\gamma_{diff} \approx \frac{3.66(2D_g)}{\bar{c}r} \quad (4)$$

where $D_g$ is the overall pressure dependant gas phase diffusion coefficient, and $\nu$ is the mean thermal velocity. The factor 3.66 is valid when axial diffusion can be neglected. This is the case in these experiments, which were characterized by Peclet numbers[29] of ≈40. The measured uptake coefficient, $\gamma_{meas}$ is obtained directly from $k_w$:

$$\gamma_{meas} = \frac{2rk_w}{\bar{c}} \quad (5)$$

If loss rates of a trace gas to the aqueous surface are rapid and irreversible, by re-arranging eqns (3) and (4), it can be shown that for diffusion limited uptake:

$$\frac{1}{\gamma_{meas}} = \frac{1}{\alpha} + \frac{\bar{c}r}{7.32 D_{TOT}} \quad (6)$$

where

$$\frac{1}{D_{TOT}} = \frac{p_{H_2O}}{D_{H_2O}} + \frac{p_{He}}{D_{He}} \quad (7)$$

**3.1.2 Uptake of HOI.** The uptake of HOI (5–50 × $10^{10}$ molecules cm$^{-3}$) to various surfaces was studied in the WWFT at UCAM. Several combinations of dissolved concentrations of $Cl^-$ and $Br^-$ in solutions of different pH were used. Uptake on pure water films was also measured. Experiments were all conducted at 274 K and at flow tube total pressures of 13 and 20 Torr. A typical result (uptake onto 2 M NaCl, 0.01 M NaBr, pH 2 solution, $P$ = 13.1 Torr) is shown in Fig. 2 that

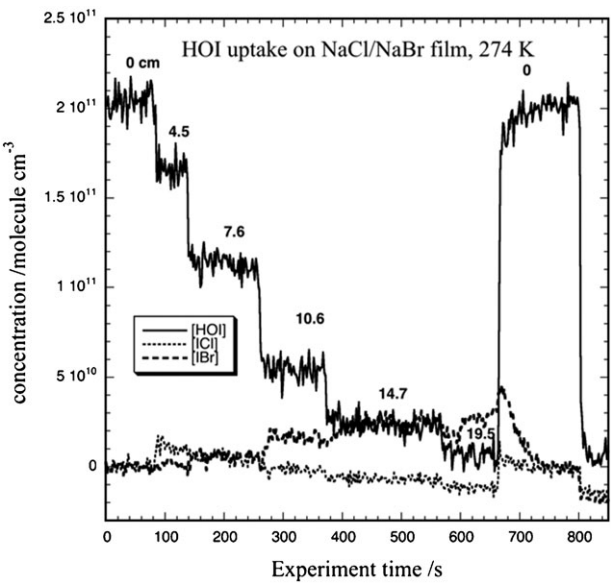


**Fig. 2** Calibrated mass spectrometer traces showing the removal of HOI (black), the formation and uptake of ICl (dotted), and the formation of IBr (grey) at different exposure lengths to aqueous film (2 M NaCl, $1 \times 10^{-2}$ M NaBr, pH = 2). Numbers show length of film exposed in cm. Temperature = 274 K; pressure = 13 Torr; gas flow speed = 176 cm s$^{-1}$.

 

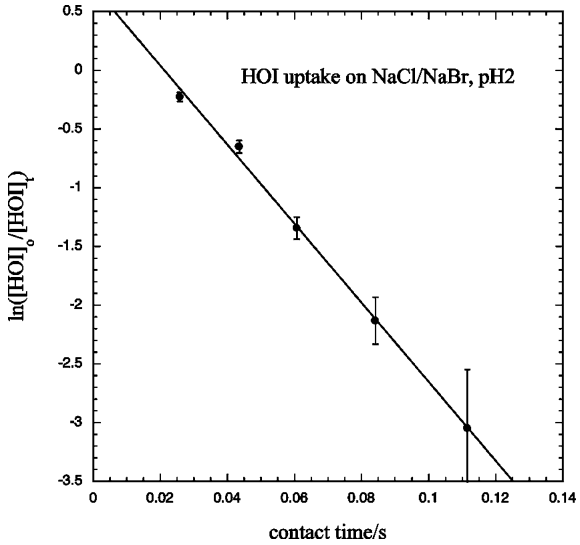


**Fig. 3** First order plot of decay of HOI exposed to 2 M NaCl, $1 \times 10^{-2}$ M NaBr, pH = 2 (data from Fig. 2). Line obtained by least squares regression analysis; slope gives $k^1 = 33.6\ s^{-1}$.

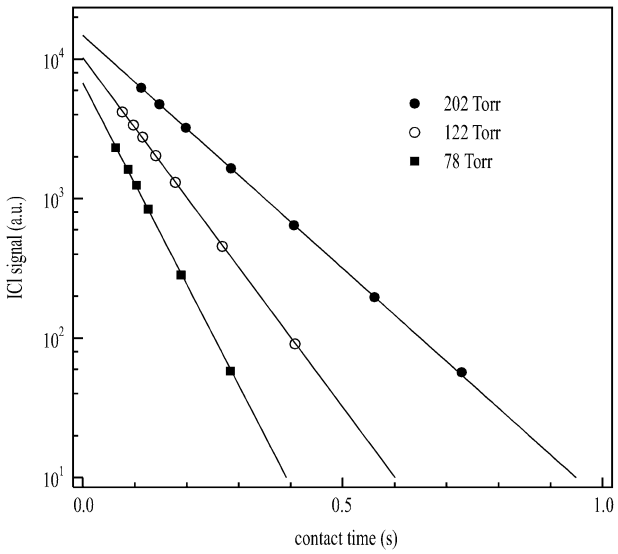


**Fig. 4** Reaction of ICl with 2 M NaBr solution: pseudo-first order decay of ICl at 278 K and 3 different pressures. Statistical errors (obtained by least squares fitting to recorded MS data) are smaller than the data symbols.

displays injector position dependent HOI signals (black trace), which decrease with contact time. There is a concurrent increase in IBr signal (dashed trace). The ICl signal (dotted trace) shows a transient increase at short exposure time and decreases at longer exposure.

Fig. 3 shows a plot of the decay in [HOI] data shown in Fig. 2 according to eqn (2), with reaction time calculated using the mean flow speed of 175 cm $s^{-1}$. The plot is linear over most of the exposure length (*i.e.* first order uptake kinetics), except in the initial section of ~4 cm where mixing of the gas stream from the sliding injector is incomplete. The first order rate coefficient was calculated from the slope of the linear portion of the plots and uptake coefficients were calculated from eqn (5).

The measured HOI uptake coefficients, $\gamma_{meas}$, are summarized in Table 2. The values given are the mean of several determinations for each set of conditions. The uptake coefficient values are close to $\gamma = 2.2 \times 10^{-3}$, independent of composition or pH of the solution, except for pure water or very low electrolyte concentration. This suggests that uptake is diffusion limited in all cases, and this was confirmed by calculations of $\gamma_{meas}$ using eqns (6) and (7) and HOI diffusion coefficients of $D_{H_2O}^{HOI} = 36.8\ cm^2\ s^{-1}\ Torr^{-1}$, and $D_{He}^{HOI} = 318.2\ cm^2\ s^{-1}\ Torr^{-1}$ at 274 K, obtained by extrapolation from the data of Holmes *et al.*[14] There was no significant difference between the $\gamma$ values at the two total pressures used, reflecting the dominant influence of $H_2O$ partial pressure on the diffusion coefficient, and hence on the diffusion limited uptake rate. The uptake rate coefficient on pure water at extended exposure times declined, giving non-first order decay, indicative of surface saturation. These results do not allow determination of the accommodation coefficient for HOI, $\alpha_{HOI}$; only a lower limit of $\alpha_{HOI} > 2.2 \times 10^{-3}$ can be deduced.

**3.1.3 Uptake of ICl.** The WWFT experiments at the MPI were conducted using ICl concentrations in the range $1–5 \times 10^{13}$ molecule $cm^{-3}$ and mostly using a 2 M bromide solution that had been acidified to pH 2 using $H_2SO_4$. Under these conditions, reaction at the surface is very rapid, and the uptake is diffusion limited. The MS signal of ICl was monitored at $m/z = 162$, and the evolution of this signal at various injector positions for a given set of conditions was recorded. In some datasets it was necessary to make a small correction for a drift in the ICl flow rate over the course of taking the data. This correction was generally less than 5%.

The pseudo-first order loss coefficient, $k_w$ was calculated from the injector position dependent signals of ICl as described by eqn (2) and plotted in Fig. 4. The ICl decay is strictly exponential over more than two orders of magnitude change in signal, indicating complete irreversibility of the uptake process.

The slopes of each dataset ($k_w$) are converted to an uptake coefficient, $\gamma_{meas}$ *via* eqn (5) using temperature dependent values of $\bar{c}$ of 19 070 cm $s^{-1}$ and 19 575 cm $s^{-1}$ at 278 and 293 K, respectively. The statistical errors on the slopes are generally less than 1%. The overall error will be larger, and associated with corrections to the raw data for drifts in the ICl signal or mass spectrometer sensitivity (see above).

The values of $\gamma_{meas}$ thus obtained lay in the range $6–16 \times 10^{-4}$, and showed a strong dependence on the experimental pressure. Assuming that gas-phase diffusion limits the uptake of ICl in these experiments, and recognising that at 278 and (especially) at 293 K a significant fraction of the total pressure in the reactor is due to water, we combine eqns (6) and (7) to derive:

$$\frac{1}{\gamma} = \frac{1}{\alpha} + \frac{\bar{c}rp_{H_2O}}{7.32D_{H_2O}} + \frac{\bar{c}r}{7.32D_{He}}P_{He} \qquad (8)$$

Thus, a plot of inverse $\gamma$ *versus* the pressure of He should give a straight line with the slope proportional to the diffusion coefficient of ICl in He, with the $x$-axis intercept containing information about the accommodation coefficient, $\alpha$, and the

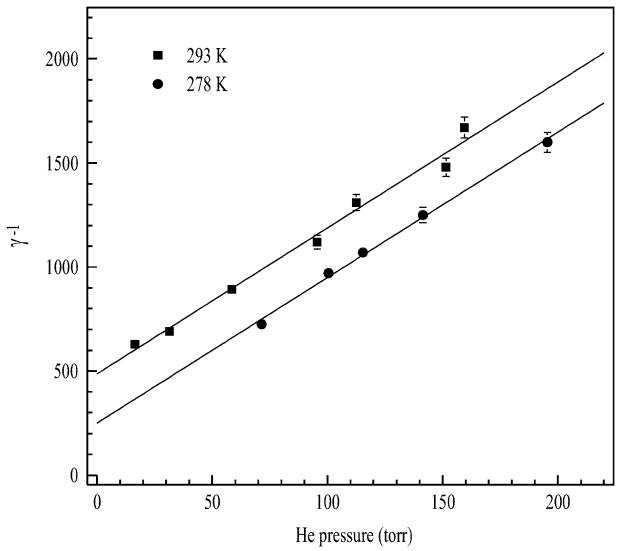


**Fig. 5** Pressure dependence of the measured uptake coefficient of ICl on 2 M NaBr solution at 278 and 293 K.

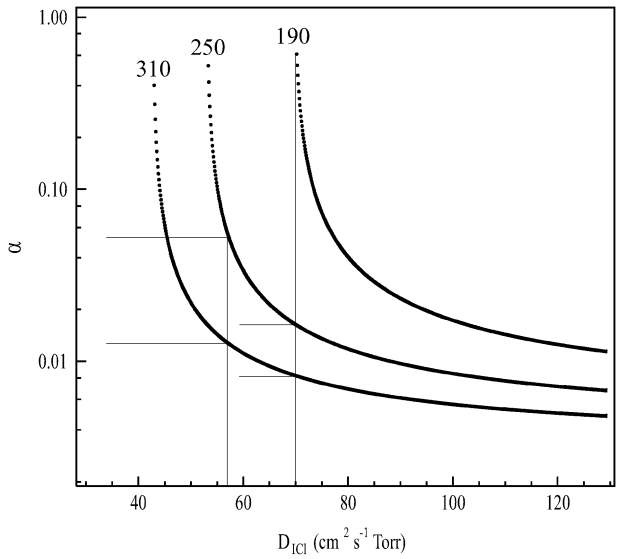


**Fig. 6** Dependence of $\alpha$ on the diffusion coeffcient of ICl in water vapour at 278 K. The solid lines labelled 190, 250 and 310 represent the central and extreme values (250 ± 60) for the intercept obtained in Fig. 5.

diffusion coefficient of ICl in water vapour. The data is plotted according to eqn (8) for the two experimental temperatures in Fig. 5. The vertical error bars take into account the effects of raw data corrections (see above).

Least squares fitting to the data in Fig. 5 yield slopes of (6.99 ± 0.46) Torr$^{-1}$ and (7.03 ± 0.36) Torr$^{-1}$ at 278 and 293 K, respectively. Using eqn (8) and the values of $\bar{c}$ presented above, we derive diffusion coefficients of ICl in He of $D_{He}^{ICl}$ (278 K) = (289 ± 19) cm$^2$ s$^{-1}$ Torr and $D_{He}^{ICl}$ (293 K) = (296 ± 15) cm$^2$ s$^{-1}$ Torr. The errors are statistical only and do not include systematic error in the value of $\bar{c}$ which was derived from the Bolzmann equation. The value of $D_{He}^{ICl}$ at 278 K is in excellent agreement with the calculation of Mössinger *et al.*[13] who derived $D_{He}^{ICl}$ (278 K) = (288 ± 32) cm$^2$ s$^{-1}$ Torr in He, and also a value of $D_{H_2O}^{ICl}$(278 K) = (57 ± 6) cm$^2$ s$^{-1}$ Torr in $H_2O$. Having established some confidence in the diffusion coefficients of ICl, we turn to the intercept values (486 ± 70) and (250 ± 60) derived by least squares fitting to data in Fig. 5. The large difference between the intercepts at 293 and 278 K is caused by the difference in the water vapour saturation pressure at these temperatures, which are 17.5 and 6.55 Torr, respectively. Taking the calculated value of the diffusion coefficient of ICl in water vapour at 278 K, and using eqn (8), we can derive a value of the accommodation coefficient, $\alpha$, of 0.05. We note that this value is derived from the difference of two large numbers, and has large, asymmetric errors associated with it. By considering only statistical errors in the size of the intercept, the value of $\alpha$ derived could be as large as 1, or as small as 0.01. This is further compounded by errors in the diffusion coefficient of ICl in water vapour, which also impact on $\alpha$. This is illustrated in Fig. 6, which shows the dependence of $\alpha$ on the value of the intercept obtained from plots of inverse $\gamma$ *versus* pressure and on the diffusion coefficient of ICl in water vapour.

The vertical lines in Fig. 6 are placed at values of $D_{H_2O}^{ICl}$(278 K) = 57 and 70 cm$^2$ s$^{-1}$ Torr, the latter being somewhat greater than the upper bound of the calculated value of (57 ± 6) cm$^2$ s$^{-1}$ Torr. The plot clearly shows that the experimental determination of $\alpha$ is subject to considerable uncertainty, with a range of $\approx$0.01 to 1 if $D_{H_2O}^{ICl}$(278 K) = 57 cm$^2$ s$^{-1}$ Torr and a range of 0.009 to 1 if $D_{H_2O}^{ICl}$(278 K) = 70 cm$^2$ s$^{-1}$ Torr. For this reason, we choose to ascribe a value of $\alpha$ = 0.01, which may be regarded as a lower limit. The equivalent calculation for the data at 293 K shows that the offset (486 ± 70) can be completely accounted for by diffusion of ICl through water vapour, removing any experimental sensitivity to the accommodation coefficient at this temperature.

A series of experiments were also conducted on ICl uptake to pure $H_2O$. At 293 K, uptake coefficients obtained were significantly lower than for the bromide solutions described above (between 5–6 × 10$^{-4}$), and also showed significantly more scatter and no obvious trend with pressure. This can be interpreted as saturation of the surface layers of the liquid film, resulting either from insufficient solubility of ICl or decrease chemical reactivity of solvated ICl in the film. Experiments in which modulation of the film thickness by variation of the liquid flow rate was carried out confirmed this, as dissolved ICl degassed from the thinner film.

In these experiments, $\gamma$ will depend on the film thickness and speed and also on the gas phase concentration of ICl, which together probably account for the observed scatter in the data.

At 278 K, the uptake coefficients measured using pure $H_2O$ were slightly lower than those measured using bromide solutions (Table 2), suggesting that, at this temperature, the solubility of ICl is sufficiently high that the uptake is quasi-irreversible. The uptake coefficients to $H_2O$ at 278 K also displayed a very similar dependence on pressure as uptake to the bromide solutions at this temperature, and resulted in a similar intercept on the plot of inverse $\gamma$ *versus* He pressure. This implies that the accommodation coefficient on pure water is similar to that on the bromide-containing surface, which

 

may be expected given the relative concentrations of $H_2O$ and $Br^-$ ions at the surface.

During experiments to examine the uptake of ICl to the 2 M bromide surfaces, the mass spectrometer also took data at $m/z = 206$, a parent ion of IBr, which was expected as aqueous phase product. A small signal of IBr, less than 5% that of ICl, was always observed but showed no dependence on the contact time. A likely explanation for the lack of observation of the expected product is that IBr has a sufficiently high solubility to prevent its escape from the aqueous film in amounts enough to be detected in the gas-phase. Indeed, the occasional observation of IBr as product was observed to coincide with the undesired breaking and drying of the flowing liquid film.

The uptake of ICl and IBr was also measured in the WWFT system at University of Cambridge on pure water and on seawater mimic (2.0 M $Cl^-$ and 0.003 M $Br^-$) solutions at 274 K and 13 Torr total pressure. The uptake of ICl was also measured on 2.0 M $Br^-$ solutions. The concentrations of ICl and IBr used in these WWFT uptake experiments were in the range 0.4–7.0 $\times$ $10^{11}$ and 0.2–1.0 $\times$ $10^{12}$ molecules $cm^{-3}$, respectively. The ICl concentrations were thus some 2 orders of magnitude lower than in the MPI experiments. These results are also summarized in Table 2.

The rate of uptake and thus the measured uptake coefficient of ICl into the salt solutions was first order in [ICl], was independent of solution pH, and was diffusion limited, with a lower limit of approximately $\gamma_{meas} > 3 \times 10^{-3}$. The results for ICl uptake were in agreement within experimental error with the results from MPI, when corrections for the different pressures and flow tube dimensions used in the two systems were taken into account. Only a limited number of studies of the uptake of IBr onto aqueous solutions were performed. The uptake was diffusion limited and the measured uptake coefficient for IBr into seawater mimic (2.0 M $Cl^-$ and 0.003 M $Br^-$) was $\gamma = 2.0 \pm 0.2 \times 10^{-3}$.

In the Cambridge apparatus the uptake of ICl and IBr onto pure $H_2O$ showed significant departure from exponential decay, with a decline in apparent $k_w$ (and hence in $\gamma_{meas}$) with exposure length. The $\gamma_{meas}$ for ICl at short exposure length was similar to that on halide solutions, was independent of [ICl], and was gas phase diffusion limited. The $\gamma_{meas}$ for IBr at short exposure length was substantially lower than the gas phase diffusion limit. Moreover, on exposure to a fresh surface, the uptake rate of IBr was time dependent, the initial larger uptake declining to the lower steady state rate, which was used to calculate $k_w$ and the cited values of $\gamma$. The observation of a time-dependent uptake rate coefficient strongly suggests saturation of the surface layer due to limited solubility or reduced rate of hydrolysis of ICl and IBr in the film. However, analysis of the data according to the resistance model for liquid diffusion-limited solubility or reaction did not reproduce the time dependence of the uptake coefficient. This may be due to turbulent mixing in the film, reducing saturation at low doses.

**3.1.4 Product release from halide films.** Product release studies were conducted in the University of Cambridge WWFT system, where the slower flow and reduced thickness of the aqueous film provided conditions favourable for the transfer of the volatile products from the liquid to the gas phase. In both the HOI and ICl uptake experiments, gas phase products were observed. However IBr uptake resulted in no observable gas phase products. For HOI, the gas-phase products released were dependent on the surface composition. In the case of a sea-salt proxy solution (2 M $Cl^-$ 1 $\times$ $10^{-2}$ M $Br^-$, pH 2) the major product was IBr with yields of up to $\sim$20% of HOI reacted. As noted above, ICl was observed but shows a transient increase at short exposure time and *decreases* at longer exposure to a value below that when the HOI is not exposed to the film. We believe this is due to ICl production from reaction of HOI with solid NaCl on the walls of the sample manifold downstream from the experimental region, which declines when [HOI] is reduced by exposure to the upstream film. The initial transient ICl increase may result from evaporation of product ICl at short exposure lengths, due to slow liquid phase reaction at these low [$Br^-$]. Uptake of HOI into 2 M NaCl solution led to small yields of gas phase ICl but no IBr.

IBr yields were measured for uptake of HOI into 2 M $Cl^-$/ 1 $\times$ $10^{-2}$ M $Br^-$ salt solution as a function of pH. The IBr yield decreased from 12 to 8% (error: $\pm$3%) when pH was changed from 2 to 5.5. Nevertheless the decrease is barely significant within the errors, which result from variabilty in measured values and uncertainty in absolute calibration. There was also an increase of $\sim$50% in the yield of IBr released as the bromide was increased from 0.01 to 0.1 M, with a fall in the yield of ICl. This observation supports the mechanism in which the relative amounts of ICl and IBr which are formed when HOI is taken up depends on the extent to which the sea salt aerosol is depleted in bromide. However because the release of dihalogens to the gas phase was non-quantitative, relative reactivity with $Br^-$ and $Cl^-$ could not be determined.

The uptake of ICl on salt solutions containing bromide at pH $<$ 7, resulted in the production of IBr. The yield of gas phase IBr (per ICl molecule taken up) was found to be 10–20% for a solution of pH 2, 2 M $Cl^-$, 1 $\times$ $10^{-3}$ M $Br^-$. This is the same within error as the yield of IBr following uptake of HOI onto films of similar halide concentration and pH. Solutions in the pH range 2–10 were used in the ICl product study, shown in Fig. 7. Under constant conditions (*e.g.* constant film speed and salinity) the yield of IBr relative to the amount of ICl taken up, decreased from 0.18 to 0 as the pH of the solution increased from 2 to 10.

As noted above, the amount of gas phase IBr observed in both the HOI and ICl WWFT uptake experiments was much less than the molar equivalent of HOI or ICl lost. The yield was also shown to decrease as a function of film thickness, suggesting that some ICl and IBr may be lost by diffusion and flow out in the bulk liquid phase. This is consistent with the observation in this and other studies that dihalogens are taken up into mobile aqueous films. In the studies of the uptake of IBr onto aqueous solutions no gas phase products were observed, in agreement with other studies on solid films.[13] The observed rapid uptake of IBr and ICl on pure water is consistent with larger partitioning into the aqueous phase compared to BrCl, $Br_2$ and $Cl_2$, reflecting their higher solubilities.[30]

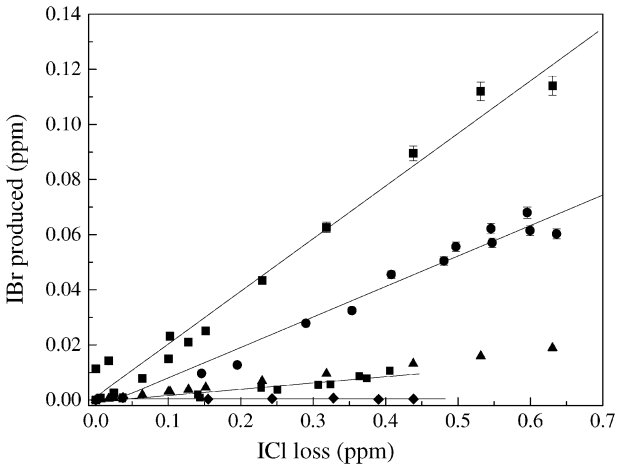


**Fig. 7** Left: IBr produced from ICl uptake as a function of solution pH. Fractional yields of IBr per ICl molecule taken up are 0.18, 0.11, 0.02 and 0 for pH 2, 5.5, 7 and 10 respectively.

**Table 3** Summary of ICl uptake onto aerosols

| RH (%) | $[Br^-]$/M | $d_{mean}$/nm | $\gamma$ | $N$ | Product |
|---|---|---|---|---|---|
| NaBr | | | | | |
| 10 | >32 | 750–2000 | $0.020 \pm 0.005$ | 3 | IBr |
| 30 | 28 | 690–2000 | $0.010 \pm 0.005$ | 3 | IBr |
| 45 | 20.1 | 370–410 | $0.010 \pm 0.007$ | 3 | IBr |
| 63 | 12.8 | 480 | $0.020 \pm 0.01$ | 1 | |
| 63 | 12.8 (pH 2) | 1760 | $0.006 \pm 0.004$ | 1 | IBr |
| 63 | 12.8 (pH 10) | 97 | $<1 \times 10^{-4}$ | 1 | no |
| 70 | 10.1 | 380 | $0.010 \pm 0.002$ | 1 | IBr |
| Sea salt | | | | | |
| 5 | >30 | 217 | $1 \times 10^{-4}$ | 6 | no |
| 30 | 18 | 310 | $3 \times 10^{-4}$ | 3 | no |
| 55 | 10.2 | 375 | $5 \times 10^{-4}$ | 1 | no |
| 87 | 3 | 479 | $1 \times 10^{-3}$ | 1 | no |
| NaCl | | | | | |
| 30 | 0 | | $<1 \times 10^{-4}$ | 1 | no |

$N$ = number of experiments.

### 3.2 ICl uptake using the AFT-CIMS

The uptake of ICl onto sodium bromide, sodium chloride and sea salt aerosol was studied with the AFT-CIMS system. The majority of the work focused on the uptake of ICl onto sodium bromide; however some experiments were performed with aerosols generated from sea salt and sodium chloride. The ICl reactant concentration was measured at the end of the flow tube for a range of reaction zone lengths corresponding to reaction time, $t$, and the first order rate coefficient, $k$, was determined from plots of ln[ICl] *vs.* $t$. In each case the decay of [ICl] was measured in the presence and absence of aerosol. The first order loss rate coefficients were corrected for diffusion and wall losses under non-plug flow conditions, using the method of Brown.[31] In the corrections the gas-phase diffusion coefficient, $D_g$, for ICl was assumed to be 0.150 $cm^2\ s^{-1}$ as calculated by extrapolation of the WWFT experimental values. The correction procedure resulted in values between 1 and 60% higher than the observed inputs. The corrected first order rate coefficient, $k^I$, was then used to determine the uptake coefficient, $\gamma$, using the aerosol surface area, $S_a$, and eqn (9) (see below). The uptake coefficients determined in this way are given in Table 3.

The rate equation for a heterogeneous reaction in a cylindrical flow tube is:

$$\frac{d[X]}{dt} = k^I[X] \quad \text{where} \quad k^I = \frac{\gamma\omega S_a}{4} \ ([X] = [ICl]) \qquad (9)$$

where $\gamma$ is the uptake coefficient, $\omega$ is the average molecular speed, $S_a$ is the surface area of the aerosol per unit gas volume. This equation assumes a monodisperse aerosol of particles small enough so that gas phase diffusion does not limit the rate of uptake. The size-averaged values of $\gamma$ obtained from eqn (9) are representative of the effective radius, *i.e.* $\gamma = \gamma(r_s)$. The effective radius is given by $r_s = 3\ V_a/S_a$ where $V_a$ is the volume of the aerosol per unit volume.

However, for polydisperse aerosols such as those used in this study, the uptake rate coefficient is an average value over the whole distribution of particles radius $r_i$, *i.e.*

$$k^1 = \sum k(r_i) = \sum_i \frac{\gamma(r_i)\omega N_i \pi r_i^2}{1 + \gamma(r_i)\left(\frac{0.75+0.283\,Kn_i}{Kn_i(Kn_i+1)}\right)} \qquad (10)$$

This equation takes into account the gas phase diffusion limitation for large particles in the term containing the Knudsen number ($Kn_i = 3D_g/\omega r_i$), as discussed by Fuchs and Sutugin[32] and Fried *et al.*[33] It also specifies a size dependence of the uptake coefficient $\gamma(r_i)$, arising, for example, from slow chemical processing in small particles, as discussed by Hanson *et al.*[34]

For the case of a size-independent uptake coefficient, we found that the value of $\gamma(r_s)$, derived by iterative solution of eqn (10), using the data from the DMA to calculate $N_i$ and using $D_g$ (ICl/$N_2$) = 0.015 $cm^2\ s^{-1}$, differs from the value of $\gamma$ obtained using eqn (9) and the total surface area, $S_a$, by <1%. We conclude that the particle radii and uptake coefficients are too small for gas phase diffusion limitations to be significant. The possible size dependence of the values of $\gamma$ ($r_s$) calculated using eqn (9) is discussed further below.

If the uptake process is driven by the reaction in solution of the ICl to form IBr, as the results suggest, then this analysis is only valid when initial $[Br^-_{(aq)}] \gg \Delta[ICl_{(g)}]$. (each in molecules $cm^{-3}$). The amounts of $Br^-$ present in the aerosol were estimated using thermodynamic data from the literature for sodium bromide,[35,36] and the measured aerosol volumes. It was found that for relative humidities 10–70%, the total $[Br^-_{(aq)}]$ per unit volume of gas was $\sim(2 \pm 1) \times 10^{14}$ molecules, *i.e.* $[10 \times \Delta[ICl_{(g)}]$. Thus the sodium bromide aerosol data fulfilled the criteria for pseudo-first order kinetics.

The bromide content of sea salt aerosol is much lower and thus failure of the strictly first order conditions was likely. Using data for RH dependence of $[Cl^-]$ for NaCl aerosol from the AIM database,[37,38] and a fixed Cl/Br molar ratio of 635, it was estimated that total aerosol [Br] was less than the average amount of ICl reacted on the aerosol. In some decays there was indication of a decline in decay rate with time. However most of the time decay was close to the wall loss, and the

 

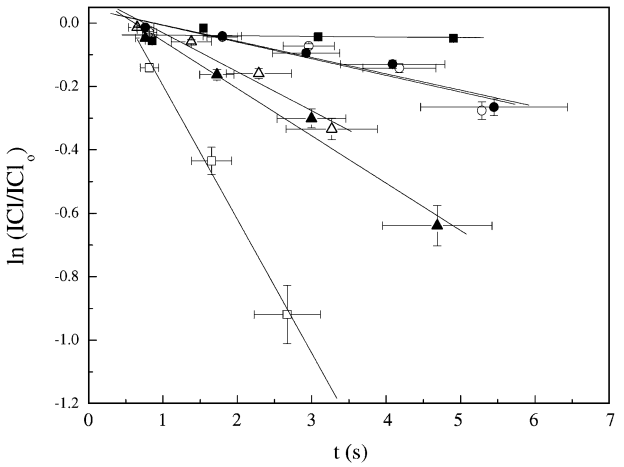


**Fig. 8** First order plot of ln ([ICl/IClo) as a function of time. (RH = 44%, 600 ppb ICl, $T$ = 274 K). Wall loss ■; NaBr aerosol surface areas ($10^{-3}$ cm$^2$ cm$^{-3}$): ● 0.7; ○ 1.0; ▲ 1.3; △ 1.6; □ 4.7.

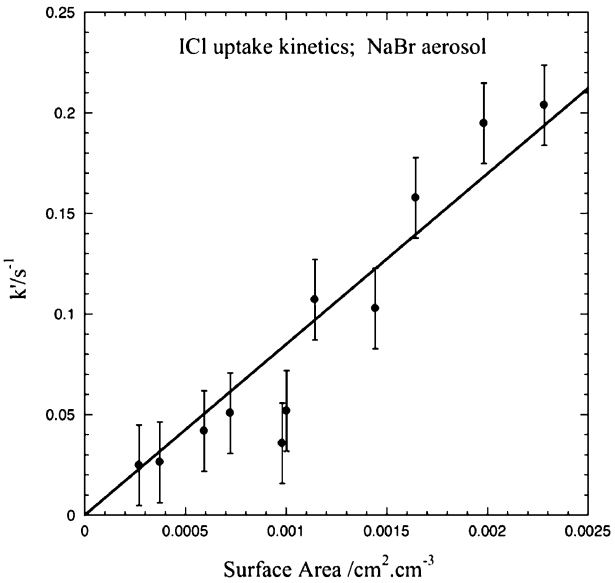


**Fig. 9** Corrected first order rate coefficient $k^I$ as a function of aerosol surface area for ICl uptake onto sodium bromide aerosol at 274 K. Solid line is a least squares fit to the data forced through the origin.

scatter in the data made it difficult to detect non-exponential decay. Thus measured uptake could not be reliably attributed to the $Br^-$ present in the sea salt aerosol.

**3.2.1 Uptake of ICl on sodium bromide.** Fig. 8 shows a plot of ln([ICl]/[ICl]$_o$) as a function of time of exposure to the aerosol, obtained with different average total surface area concentrations of aqueous sodium bromide aerosol at 44% relative humidity and with initial [ICl] = $8 \times 10^{12}$ molecule cm$^{-3}$. The decay due to wall loss, measured in the absence of aerosol is also shown. The uptake onto the aerosol is substantially faster than wall loss. The relatively large error bars on the time axis result from the fluctuation in the flow rate arising from aerosol deposition in the orifice at the exit of the flow tube. The corrected first-order rate coefficients, $k^I_{corr}$, are plotted as a function of surface area concentration in Fig. 9. The error bars represent uncertainty in both the aerosol surface area and the corrected $k^I_{corr}$ on the $x$- and $y$-axes, respectively. The uptake rates are clearly proportional to aerosol surface area.

Uptake coefficients for ICl onto aerosols made from neutral aqueous sodium bromide and also pH-adjusted solutions are shown as a function of RH in Fig. 10. For the neutral solutions it can be seen that the uptake coefficient is invariant with RH over the range studied within the experimental error. The average uptake coefficient of the results is 0.018 ± 0.004. For acidic aerosol (pH 2), a barely significant reduction of the uptake coefficient was observed (grey square, Fig. 10), but experiments using pH 10 aerosols showed very low ICl uptake, close to the limit of detection, with $\gamma \sim 1 \times 10^{-4}$. The uptake coefficient for ICl uptake onto effloresced sodium bromide aerosol was significantly lower than deliquesced sodium bromide aerosol, $\gamma = (6 \pm 4) \times 10^{-3}$ (RH = 5%). However due to the limited availability of NaBr on the surface of the aerosol particles it is likely that in these experiments the conditions are not under pseudo-first order conditions with respect to the ICl : $Br^-$ ratio. These results for dry aerosols are consistent with those of Mossinger and Cox,[13] who measured an uptake coefficient to a fresh sodium bromide powder surface at 11% RH of $\gamma$ = 0.030, which decreased, as the surface was aged, to $\sim 8 \times 10^{-3}$.

Upon uptake of ICl, IBr is released into the gas phase in the cases of the neutral, acidified and solid sodium bromide aerosols. This result is similar to the observations made in the WWFT study reported in this work. The production of IBr is directly proportional to the uptake of ICl, (Fig. 11), except for a delay at small extent of reaction. The average yield is 0.6 ± 0.3, *i.e.* substantially higher than from uptake onto the bulk film. The large error bars are due to the scatter in the data and the uncertainties associated with the IBr and ICl calibrations. No IBr release was observed for alkaline (pH 10) aerosols. This could be attributed to a change in mechanism in the basic solution. $IO^-$ can be formed from the reaction sequence:

$$ICl + H_2O \leftrightarrow HOI + Cl^- + H^+ \quad (R12)$$

$$HOI \leftrightarrow H^+ + IO^- \quad (R13)$$

Iodate can then be formed from the disproportionation of HOI, competing with the formation of IBr. Disproportionation of HOI to iodate and iodide at high pH has been studied both experimentally and theoretically.[39–41] The overall reaction can be given by

$$3HOI \rightarrow IO_3^- + 2I^- + 3H^+ \quad (R14)$$

Below pH 5 the disproportionation is not thermodynamically favoured.

**3.2.2 Uptake of ICl onto sea salt aerosol.** In experiments with sea salt aerosol, much smaller uptakes than those seen with sodium bromide were observed. In many cases the uptake

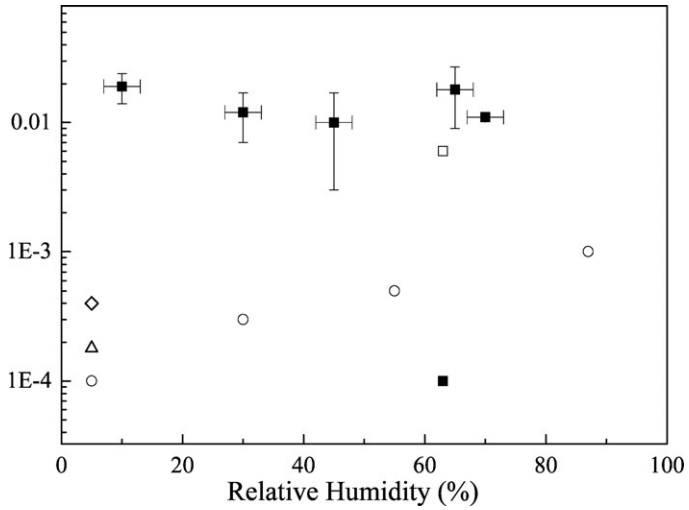


**Fig. 10** Uptake coefficients as a function of relative humidity for sodium bromide (neutral: black squares, pH 2: open square, pH 10: filled square), sea salt (○) and solid sodium bromide (◇) and sodium chloride (△) aerosol.

rate onto aerosol was not significantly higher than the wall loss. Uptake coefficients obtained from experiments in which the aerosol uptake was larger than the wall loss are shown in Table 3 and Fig. 10. Since these values were measured in reactant-limited experimental conditions the uptake coefficients may not be solely attributable to reaction with $Br^-$. However it can be seen that uptake is an order of magnitude slower than on NaBr and there is a distinct decline of $\gamma$ with decreasing RH. This suggests that chemical reaction in the particles is controlling the uptake rate. Only very small increases in the IBr signals were observed during uptake, generally just above the level observed normally in baseline signal drift. This was consistent with the small amount of $Br^-$ present in the aerosol. When aerosols of pure sodium chloride were present ICl decay was not significantly higher than wall loss, with $\gamma < 1 \times 10^{-4}$.

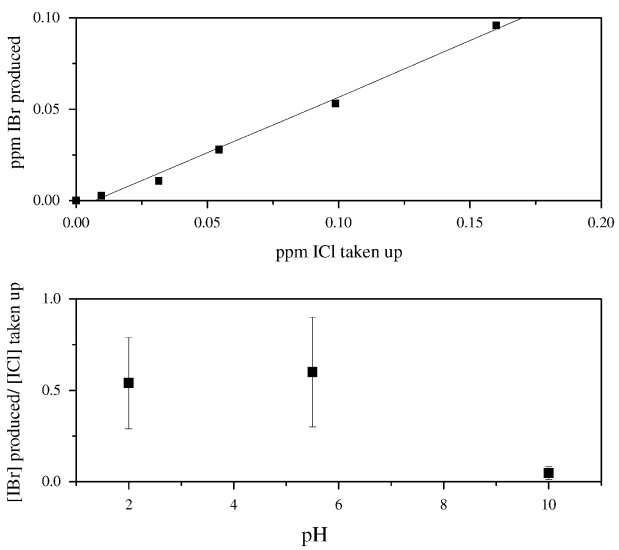


**Fig. 11** IBr production: upper panel: ppm IBr produced as a function of ppm ICl taken up; lower panel: fractional yield of IBr per ICl taken up as a function of aerosol solution pH.

## 4. Discussion

### Uptake of HOI

The uptake of HOI into aqueous solutions is clearly rapid. The rate of uptake onto the bulk films of halide salts and pure water was diffusion limited. There was some indication of surface saturation on pure water as the uptake rate declined after long exposure to high [HOI]. Experimental constraints did not allow measurements of uptake of HOI as a function of pressure (to characterise the diffusion loss rate), or onto aerosols, and so the results obtained here do not allow determination of the accommodation coefficient or reactive uptake coefficient for HOI, and set a lower limit of $\alpha \gg 3 \times 10^{-3}$, the diffusion limited uptake coefficient. A lower limit of $\alpha = 0.3$ for HOI on aqueous sulfuric surfaces was reported by Holmes *et al.*,[14] and Wachsmuth *et al.*[42] report $\alpha = 0.6$ for HOBr on aqueous NaBr aerosols. Thus it is highly likely that the accommodation coefficient of HOI on aqueous surfaces is $>0.3$ at ambient temperatures. Following uptake into halide salt solutions, HOI reacts with $Cl^-$ or $Br^-$ to form ICl or IBr. Although the rate constant for reaction of HOI with $Br^-$ is faster than with $Cl^-$ by a factor of 114; [43,44] ICl is expected to be the major initial aqueous phase product in fresh sea salt aerosol. However even when quite small amounts of $Br^-$ are present, ICl is converted in solution to IBr, which is the main gas-phase product observed. Under the conditions of the WWFT experiments the yield of IBr relative to the amount of HOI taken up is only $\sim$20%; it is probable that the balance remains in solution and is removed in the flowing aqueous film. This yield contrasts to that observed with the reactive uptake of HOBr, investigated under similar conditions in a WWFT, where the total yield of gas-phase $Br_2$ or BrCl products is stoichiometric, reflecting the lower solubility of these dihalogens.[15]

### Uptake of ICl

Measurements of ICl uptake onto aqueous film sea salt proxies, as well as onto pure water, show that ICl has quite

 

high solubility and reacts with $Br^-$. The uptake rate is gas-phase diffusion limited and the diffusion coefficients and accommodation coefficient have been determined from the pressure dependence of the uptake coefficients. An accommodation coefficient of $\sim$0.05 has been obtained, with a large uncertainty covering the range 0.01–1.0, arising from the uncertainty in the values of $D_g$. The uptake of ICl on solutions containing $Br^-$ led to gas-phase IBr with a similar yield to that from HOI uptake on films with the same composition, the amounts released being limited by mass transfer into the bulk.

Uptake of ICl into Br-containing aerosols was also studied with a view to avoiding the diffusion and solubility limitations. In the AFT-CIMS experiment the mean uptake coefficient of ICl onto deliquescent particles of sodium bromide was $\gamma = 0.018 \pm 0.004$, invariant with relative humidity between 10 and 70%. IBr was released to the gas phase with a yield of $0.6 \pm 0.3$ per molecule ICl reacted, although taking account of the uncertainty of the calibrations and the experimental error, the yield could in reality be close to unity.

Since the concentration of $Br^-$ in the bulk aqueous phase changes by approx. a factor of 3 over the RH range (see Table 3), the constant value for $\gamma$ suggests that uptake is accommodation controlled, as opposed to chemically controlled. The measured value of $\gamma = 0.018$ is consistent with the range suggested for the accommodation coefficient for ICl uptake based on the WWFT experiments (0.01–1.0), although lower than the best estimate from the analysis of $\alpha_{ICl} = 0.05$. Therefore chemical resistance cannot be ruled out. Using the above values of $\gamma$ and $\alpha$ and assumed values of $H(ICl) = 110$ M atm$^{-1}$ [45] and $D_l^{ICl} = 0.5 \times 10^{-5}$ cm$^2$ s$^{-1}$ at 274 K, in eqn (11):

$$\frac{1}{\gamma} = \frac{1}{\alpha} + \frac{c}{4RTH(D_l k_{het})^{0.5}} \qquad (11)$$

a lower limit value of $k_{het}$ can be derived. The results give $k_{het} \sim 600$ s$^{-1}$ and the corresponding reacto-diffusive length ($=\sqrt{(D_l/k_{het})}$) of 1080 nm; this is larger than the typical aerosol particle radius, and should have resulted in size dependent uptake coefficients. There was no significant correlation between the aerosol size and measured $\gamma$ values for the NaBr aerosol and it is therefore concluded that $k_{het} \gg 600$ s$^{-1}$ and uptake was accommodation controlled. Therefore $\gamma = \alpha = 0.018 \pm 0.004$.

The much lower uptake coefficients observed for the sea salt aerosol can be attributed to reduced rate of chemical reaction of ICl in the aerosol because of the much lower [$Br^-$]. The concentration of $Br^-$ initially present in the aerosol, was calculated assuming a constant [Br]/[Cl] ratio of $1.55 \times 10^{-3}$, and using [$Cl^-$] values at a given RH from the AIM thermodynamic database. These values are given in Table 3. The average [$Br^-$] present will be at least a factor of 2 lower due to depletion by reaction with ICl taken up. The uptake coefficients show a distinct increase with particle size ($V/S$) indicating volume limited uptake kinetics. Rate constants for liquid phase reaction were derived from the measured $\gamma$ values using the appropriate form of the resistance model equation, together with $\alpha = 0.018$:

$$\frac{1}{\gamma} = \frac{1}{\alpha} + \frac{c}{4RTH(V/S)k_{het}} \qquad (12)$$

The values of $k_{het}$ increased from 55 to 250 s$^{-1}$ over the RH range 5–87%, whilst the [$Br^-$] showed the opposite trend. Clearly the uptake of ICl in these experiments was not controlled by $Br^-$ reaction, as expected, since the total amount of $Br^-$ in the aerosol was less than the ICl reacted. The chemistry leading to slow ICl uptake into these aged sea salt particles is unknown. Solubility is insufficient to account for loss of ICl to the particles.

### Mechanism of the reaction

The results from this study confirm suggestion that HOI can lead to production of dihalogens from neutral or acidic halide solutions, following its reaction with $Cl^-$ or $Br^-$, in the same manner as has been found for HOBr. They also show that production of IBr is favoured over ICl, such that IBr is the predominant product even at [Br]/[Cl] $< 10^{-3}$. The higher solubility of ICl and IBr,[43] compared to $Cl_2$, $Br_2$ and BrCl, led to retention of these products in the bulk film of the WWFT experiments, and did not allow quantitative measurements of the relative rates of ICl and IBr production in solution. In particular, ICl release from the films could only be observed at short exposure times. However the results for the uptake of ICl on aerosols showed that IBr is rapidly produced from ICl in Br-containing solution, and is efficiently released to the gas phase. Since HOI reacts with $Cl^-$ to form ICl it can act as a catalyst for activation of Br from sea-salt aerosols, *via* the reactions:

$$HOI_{aq} + Cl^-_{aq} + H^+_{aq} \rightarrow ICl_{aq} + H_2O_l \qquad (R7)$$

$$ICl_{aq} + Br^-_{aq} \rightarrow IBr_{aq} + Cl^-_{aq} \qquad (R10)$$

$$IBr + h\nu \rightarrow Br + I \qquad (R11)$$

$$I + O_3 \rightarrow IO + O_2 \qquad (R4)$$

$$IO + HO_2 \rightarrow HOI + O_2 \qquad (R1)$$

It is worth briefly considering the atmospheric implications of these results. From the experiments presented here and elsewhere, it is possible to calculate an uptake coefficient for HOI onto seawater using the resistance model equations. On small particles it will be accommodation controlled with $\alpha \sim 0.3$; on particles $>3$ μm uptake will be gas phase diffusion controlled ($\gamma \sim 0.1$). Bromine depletion is a widely observed phenomenon in sea salt aerosol. On average, about 50% of bromide in sea salt aerosol is depleted,[10] (bromine depletion factor, $DF = 50\%$), which makes sea salt a potentially large bromine source to the atmosphere.[46]

An IBr production rate can be calculated by taking a background marine aerosol surface area ($1.8 \times 10^{-5}$ cm$^2$ cm$^{-3}$, Bates *et al.*[47]) a modelled ambient HOI concentration, ([HOI] $= 5 \times 10^7$ molec cm$^{-3}$ Vogt *et al.*[8]) and a 100% yield of IBr (not unreasonable over the longer timescales in the atmosphere). An IBr production rate of $1.4 \times 10^4$ molecule cm$^{-3}$ s$^{-1}$ is calculated. Using the submicron marine aerosol volume[43] and 64 mg l$^{-1}$ $Br^-$ in seawater, under conditions in which HOI is not depleted from the gas phase, uptake and subsequent reaction of HOI could deplete the aerosol bromide by approximately 8% in 12 h. Moreover the HOBr produced from the activated Br can itself react with sea salt aerosol to

produce further $Br_2$. This implies that HOI uptake could trigger a significant fraction of the observed bromide depletion in marine aerosol.

The results suggest that HOI-induced Cl activation as ICl from sea salt aerosol is less likely to be important. Br has to be very substantially depleted before ICl release to the gas phase can occur. Thus the value of $f = 0.5$ for the fractional conversion of HOI to gaseous ICl in a mixed-age MBL aerosol assemblage, assumed by McFiggans *et al.*,[7] is likely to give an overestimate of Cl activation, at least for the first few hours of processing of the aerosol. Subsequently the value of $f = 0.5$ may be appropriate for activation, but any ICl formed in the presence of $Br^-$-containing aerosol will have a lifetime of only 10 min. with respect to heterogeneous conversion to IBr on background marine aerosol, using the maximum uptake coefficient of 0.018 measured in this work.

## Acknowledgements

CFB would like to thank Dr Paul Griffiths and Dr Claire Badger for assistance particularly with the DMA. This work was funded in part by NERC COSMAS core strategic programme (GST/03/2718), and the EU 5th Framework Programme, THALOZ project(EVK2-CT-2001-00104).

## References

1 B. J. Allan, G. McFiggans, J. M. C. Plane and H. Coe, *J. Geophys. Res., [Atmos.]*, 2000, **105**, 14363–14369.
2 B. Alicke, K. Hebestreit, J. Stutz and U. Platt, *Nature*, 1999, **397**, 572–573.
3 F. Wittrock, R. Muller, A. Richter, H. Bovensman and J. Burrows, *Geophys. Res. Lett.*, 2000, **2**, 1471–1474.
4 D. Bauer, T. Ingham, S. A. Carl, G. K. Moortgat and J. N. Crowley, *J. Phys. Chem. A*, 1998, **102**, 2857–2864.
5 D. M. Rowley, J. C. Mossinger, R. A. Cox and R. L. Jones, *J. Atmos. Chem.*, 1999, **34**, 137–151.
6 D. Davis, J. Crawford, S. Liu, S. A. McKeen, A. Bandy, D. Thornton, F. Rowland and D. J. Blake, *J. Geophys. Res., [Atmos.]*, 1996, **101**, 2135–2147.
7 G. McFiggans, R. A. Cox, J. C. Mossinger, B. J. Allan and J. M. C. Plane, *J. Geophys. Res., [Atmos.]*, 2002, **107**, DOI: 10.1029/2001JD000383.
8 R. Vogt, R. Sander, R. von Glasow and P. J. Crutzen, *J. Atmos. Chem.*, 1999, **32**, 375–395.
9 K. L. Foster, R. A. Plastridge, J. W. Botttenheim, P. B. Shepson, B. J. Finlayson-Pitts and C. W. Spicer, *Science*, 2001, **291**, 471–474.
10 R. Sander, W. C. Keene, A. A. Pszenny, R. Arimoto, G. P. Ayers, E. Baboukas, J. M. Cainey, P. J. Crutzen, R. A. Duce, G. Honniger, B. J. Huebert, W. Maenhaut, N. Mihalopoulos, V. C. Turekian and R. Van Dingenen, *Atmos. Chem. Phys.*, 2003, **3**, 1301–1336.
11 L. J. Carpenter, *Chem. Rev.*, 2003, **103**, 4953–4962.
12 J. W. Adams and R. A. Cox, *J. Phys. IV*, Grenoble, France, 2002.
13 J. C. Mossinger and R. A. Cox, *J. Phys. Chem. A*, 2001, **105**, 5165–5177.
14 N. S. Holmes, J. W. Adams and J. N. Crowley, *Phys. Chem. Chem. Phys.*, 2001, **3**, 1679–1687.
15 S. Fickert, J. W. Adams and J. N. Crowley, *J. Geophys. Res., [Atmos.]*, 1999, **104**, 23, 719–723, 727.
16 G. Deiber, C. George, S. Le Calve, F. Schweitzer and P. Mirabel, *Atmos. Chem. Phys.*, 2004, **4**, 1291–1299.
17 L. T. Chu, G. Diao and L. Chu, *J. Phys. Chem. B*, 2002, **106**, 5679–5688.
18 Y. Bedjanian, G. Le Bras and G. Poulet, *Int. J. Chem. Kinet.*, 1998, **30**, 933–940.
19 E. Allanic and M. J. Rossi, *J. Geophys. Res., [Atmos.]*, 1999, **104**, 18689–18696.
20 J. P. D. Abbatt, *Geophys. Res. Lett.*, 1996, **23**, 1681–1684.
21 W. L. Chameides and A. Stelson, *J. Geophys. Res., [Atmos.]*, 1992, **97**, 20565–20580.
22 A. A. Pszenny, J. Moldanova, W. C. Keene, R. Sander, J. R. Maben, M. Martinez, P. J. Crutzen, D. Perner and R. G. Prinn, *Atmos. Chem. Phys.*, 2004, **4**, 147–168.
23 R. Von Glasow and R. Sander, *Geophys. Res. Lett.*, 2001, **28**, 247–250.
24 S. Fickert, F. Helleis, J. W. Adams, G. K. Moortgat and J. N. Crowley, *J. Phys. Chem. A*, 1998, **102**, 10689–10696.
25 C. L. Badger, I. George, P. T. Griffiths, C. F. Braban, R. A. Cox and J. P. D. Abbatt, *Atmos. Chem. Phys.*, 2006, **6**, 755–768.
26 S. T. Martin, *Chem. Rev.*, 2000, **100**, 3403–3453.
27 D. J. Cziczo, J. B. Nowak, J. H. Hu and J. P. D. Abbatt, *J. Geophys. Res., [Atmos.]*, 1997, **102**, 18843–18850.
28 C. Guimbaud, F. Arens, L. Gutzwiller, H. W. Gaggler and M. Ammann, *Atmos. Chem. Phys.*, 2002, **2**, 249–257.
29 A. Zasypkin, V. M. Grigor'eva, V. N. Korchak and Y. M. Gershenson, *Kinet. Catal.*, 1997, **38**, 772–781.
30 R. Sander, Compilation of Henry's law constants for inorganic and organic species of potential importance in environmental chemistry(version 3), http://www.mpch-mainz.mpg.de/~sander/res/henry.html, 1999.
31 R. L. Brown, *J. Res. Natl. Bur. Stand. (U. S.)*, 1978, **83**, 1–8.
32 N. A. Fuchs and A. G. Sutugin, *Highly dispersed aerosols*, Ann Arbor Science, Ann Arbor MI, 1970.
33 A. Fried, B. E. Henry, J. G. Calvert and M. Mozurkewich, *J. Geophys. Res., [Atmos.]*, 1994, **99**, 3517–3532.
34 D. R. Hanson, A. R. Ravishankara and S. Solomon, *J. Geophys. Res., [Atmos.]*, 1994, **99**, 3615–3629.
35 D. Lide, *CRC Handbook of Chemistry and Physics.*
36 M. D. Cohen, R. C. Flagan and J. H. Seinfeld, *J. Phys. Chem. A*, 1987, **91**, 4563.
37 K. S. Carslaw, S. L. Clegg and P. Brimblecombe, *J. Phys. Chem.*, 1995, **99**, 11557–11574.
38 A. S. Wexler and S. L. Clegg, *J. Geophys. Res., [Atmos.]*, 2002, **107**, art. no. 4207.
39 S. D. Jones and V. W. Truesdale, *J. Hydrol.*, 1996, **179**, 67–86.
40 V. W. Truesdale, *J. Chem. Soc., Faraday Trans.*, 1997, **93**, 1909–1914.
41 V. W. Truesdale and C. Canosa-Mas, *J. Chem. Soc., Faraday Trans.*, 1995, **91**, 2269–2273.
42 M. Wachsmuth, H. W. Gäggeler, R. von Glasow and M. Ammann, *Atmos. Chem. Phys.*, 2002, **2**, 121–131.
43 R. C. Troy, M. D. Kelly, J. C. Nagy and D. W. Margerum, *Inorg. Chem.*, 1991, **30**, 4838–4843.
44 Y. L. Wang, J. C. Nagy and D. W. Margerum, *J. Am. Chem. Soc.*, 1989, **111**, 7838–7842.
45 D. D. Wagman, W. H. Evans, V. B. Parker, R. H. Schumm, I. Halow, S. M. Bailey, K. L. Churney and R. L. Nuttall, *J. Phys. Chem. Ref. Data*, 1982, **11**.
46 X. Yang, R. A. Cox, N. Warwick, J. A. Pyle and G. Carver, *J. Geophys. Res., [Atmos.]*, 2005.
47 T. S. Bates, P. K. Quinn, D. S. Covert, D. J. Coffman, J. E. Johnson and A. Wiedensohler, *Tellus*, 2000, **52B**, 258–272.

 